JACS
JOURNAL OF THE AMERICAN CHEMICAL SOCIETY
Communication
pubs.acs.org/JACS

Graphene Oxide Wrapping on Squaraine-Loaded Mesoporous Silica Nanoparticles for Bioimaging

Sivaramapanicker Sreejith,[†,§] Xing Ma,[‡,§] and Yanli Zhao*[,†,‡]

[†]Division of Chemistry and Biological Chemistry, School of Physical and Mathematical Sciences, Nanyang Technological University, 21 Nanyang Link, 637371 Singapore

[‡]School of Materials Science and Engineering, Nanyang Technological University, 50 Nanyang Avenue, 639798 Singapore

Supporting Information

ABSTRACT: Squaraine dyes were loaded inside mesoporous silica nanoparticles, and the nanoparticle surfaces were then wrapped with ultrathin graphene oxide sheets, leading to the formation of a novel hybrid material. The hybrid exhibits remarkable stability and can efficiently protect the loaded dye from nucleophilic attack. The biocompatible hybrid is noncytotoxic and presents significant potential for application in fluorescence imaging in vitro.

Graphene oxide (GO) is an oxidized derivative of graphene that has a 2D carbon honeycomb lattice.[1] The presence of functional groups and sp^2-conjugated bonds on the surface of GO offers strong hydrophilic characteristics and the feasibility of $\pi-\pi$ interactions with aromatic molecules, providing excellent capacities for further functionalizations on the surface.[2] Because of the biocompatibility and low cytotoxicity of GO,[3] GO−biomolecule conjugates and GO−nanoparticle hybrids have recently been used for biological applications such as DNA detection,[4] cell imaging,[5] and drug loading/delivery.[6]

On the other hand, mesoporous silica nanoparticles (MSNPs) have been studied extensively as drug delivery platforms because of their versatility and low cytotoxicity.[7] The advantages of MSNPs, such as large internal surface areas and uniform mesopores, have attracted tremendous attention directed toward their applications for controlled drug delivery.[8] Accordingly, significant research effort has centered on developing multifunctional MSNPs for biolabeling[9] and therapeutic uses.[8a,10] Thus, the combination of the excellent properties of GO and MSNPs may generate a new research avenue for biological applications.

Squaraine dyes are a class of extensively studied zwitterionic dyes that exhibit excellent photophysical properties in the near-IR (NIR) region.[11] Squaraines have proved to be suitable for many biological applications, such as metal ion sensing,[12] NIR fluorescent labeling,[13] two-photon absorption,[14] and detection and estimation of thiol-containing amino acids.[15,16] Recent work demonstrated that these dyes can serve as the second generation of photosensitizers for photodynamic therapy (PDT).[17] However, there are two major challenges in using these dyes for biological applications, especially for PDT and imaging applications: preventing easy formation of dye aggregates in aqueous environments and protecting the photophysical characteristics from nucleophilic attack on the squaryl rings. Although approaches such as (i) supramolecular encapsulation using macrocyclic host molecules (e.g., β-cyclodextrin[18] and serum albumins[19]) and (ii) the formation of squaraine-derived rotaxanes[20] can enhance their stability and prevent chromophore interactions, the real bottleneck in maintaining the photophysical characteristics of these dyes in aqueous environments remains unresolved. In this context, the design of a suitable vessel that can completely prevent nucleophilic attack on the squaraine dyes and control the bleaching of their photophysical properties is of prime importance.

Herein we describe a novel strategy for the fabrication of GO-enwrapped MSNPs as protective vessels for the squaraine dyes. We selected for our experiments the model squaraine dye bis(2,4,6-trihydroxyphenyl)squaraine dye (**1**). The present strategy involves loading of **1** into the MSNPs followed by wrapping of GO around the surfaces of the MSNPs via electrostatic interactions (Scheme 1). The resulting GO−MSNP1 hybrid exhibits remarkable stability and complete resistance toward nucleophiles such as cysteine (Cys) and glutathione (GSH) in aqueous environments.

The electrostatic interaction of GO with metal NPs has previously been utilized for the preparation of fluorescent

Scheme 1. Preparation of GO-Enwrapped, Dye-Loaded MSNPs (GO−MSNP1)[a]

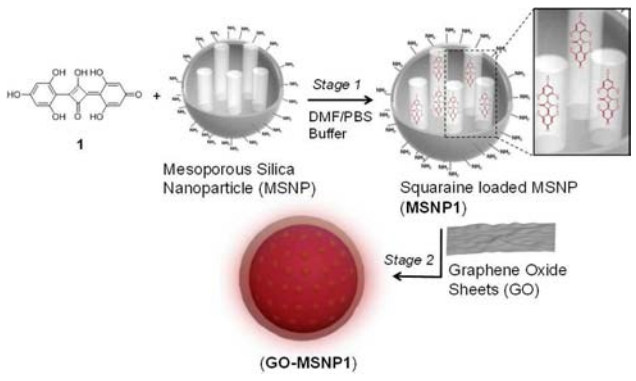

[a]Stage 1: loading of **1** in APTES-modified MSNPs. Stage 2: electrostatic wrapping of GO sheets on the surfaces of **1**-loaded MSNPs.

Received: June 3, 2012
Published: July 16, 2012

   dx.doi.org/10.1021/ja305352d | J. Am. Chem. Soc. 2012, 134, 17346−17349

hybrids and anode materials. For example, Yang et al.[21] recently reported the fabrication of GO-encapsulated metal oxide NPs as high-performance anode materials through the coassembly of GO sheets and positively charged oxide NPs. Although it would be challenging, we envisioned that the immobilization of GO sheets on MSNPs could completely cover the mesopores of the NPs. This approach would open up a novel methodology for the protection of dyes such as squaraines from both self-aggregation and nucleophilic attack. Loading of **1** into the mesopores of MSNPs followed by wrapping with GO sheets would lead to a new hybrid material, GO−MSNP1, for further applications (Scheme 1).

GO was synthesized from natural graphite powder by a modified Hammer's method[22] and converted to GO−COOH (termed GO sheets) based on previously reported procedures [see the Supporting Information (SI)].[23] The readily synthesized GO sheets were found to be dispersible in aqueous and organic solvents such as *N*,*N*-dimethylformamide (DMF). The freshly prepared GO sheets were characterized using transmission electron microscopy (TEM) (Figure S1 in the SI) and FT-IR spectroscopy (Figure S2). The TEM image (Figure S1a) shows multilayer GO sheets, and the selected-area electron diffraction (SAED) pattern (Figure S1b) also reveals the well-arranged multilayer GO sheets. Moreover, the presence of −COOH groups on the GO sheets was evident from the peaks corresponding to the C═O stretching vibration at 1726 cm^{-1} and the C−O stretching vibration at 1060 cm^{-1} (Figure S2). **1** was prepared by the condensation of 3,4-dihydroxycyclobut-3-ene-1,2-dione (squaric acid) with 2 equiv of phloroglucinol in acetic acid. The dye was purified by repeated crystallization, obtained in 58% yield, and characterized by NMR and FT-IR spectroscopy and mass spectrometry.[24] The UV/vis spectrum of **1** in 1:1 (v/v) DMF/H_2O at pH 6.5 shows two bands at 569 nm ($\varepsilon = 1.3 \times 10^5$ M^{-1} cm^{-1}) and 502 nm (Figure S3). The emission spectrum of **1** exhibits a maximum at 596 nm (λ_{ex} = 580 nm) (Figure S3).

3-Aminopropyltriethoxysilane (APTES)-modified MSNPs (MSNP−NH_2) were prepared via a cocondensation method based on previously reported procedures,[25] washed with MeOH and distilled H_2O, and dried in vacuum at 80 °C for 24 h. The NPs were then characterized by high-resolution TEM (HR-TEM) and field-emission scanning electron microscopy (FE-SEM). Figure 1a shows the HR-TEM image of MSNP−NH_2 with clear mesoporous structures. Powder X-ray diffraction (PXRD) analysis revealed a hexagonal arrangement of the mesopores, and the d_{100} spacing was calculated to be 4.16 nm using Bragg's law and the (100) position at $2\theta = 2.11°$ (Figure S4). The surface area and porous nature of MSNP−NH_2 were characterized by N_2 adsorption/desorption measurements. A typical type-IV isotherm (Figure S5) indicative of mesoporous structures was observed, with a Brunauer−Emmett−Teller (BET) surface area of 731.4 m^2 g^{-1}. The Barrett−Joyner−Halenda (BJH) mesopore size distribution based on the desorption data was sharply focused on 2.71 nm. The thickness of the mesopore walls was estimated as 1.45 nm from the difference between average internal pore size obtained from the BJH method and the average external pore size calculated from the PXRD data.

To prepare GO-sheet-encapsulated MSNPs (GO−MSNP), MSNP−NH_2 (5 mg) was suspended in DMF (1 mL) by bath sonication. A GO suspension in DMF (4 mL) was added to the MSNP−NH_2 solution, and the mixture was stirred at room temperature for 24 h to complete the electrostatic wrapping process. The GO−MSNP product was then collected by centrifugation at 8000 rpm and thoroughly washed with DMF to remove any suspended GO residues. TEM analysis of GO−MSNP (Figure 1b) revealed the successful wrapping of MSNPs with ultrathin GO sheets.

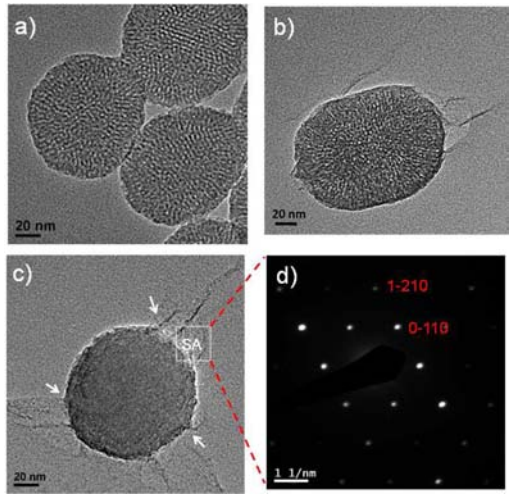

Figure 1. (a−c) HR-TEM images of (a) APTES-modified MSNPs (MSNP−NH_2), (b) GO-enwrapped MSNPs without dye loading (GO−MSNP), and (c) GO-enwrapped, squaraine-loaded MSNPs (GO−MSNP1). The white arrows in (c) indicate monolayer GO sheets. (d) SAED pattern of (c), showing ultrathin layers of GO sheets.

Inspired by the above-mentioned process, we extended the wrapping process to **1**-loaded MSNPs. A well-dispersed MSNP−NH_2 suspension in DMF (1 mL) was mixed with **1** (3×10^{-4} M) in 1:1 DMF/H_2O (0.5 mL) at pH 6.5 in a 5 mL glass vial. The mixture was stirred at room temperature for 24 h to load **1** into the mesopores of the NPs. The suspension was then centrifuged twice at 8000 rpm and the supernatant removed to obtain **1**-loaded MSNPs (MSNP1, ca. 2.5 wt % loading of **1** relative to MSNPs). After addition of a GO suspension (1 mL in DMF) to MSNP1 followed by a gentle bath sonication for 2 min, the mixture was stirred for 24 h to ensure the completion of the wrapping process. The product was then centrifuged at 8000 rpm for 30 min and washed with DMF five times to remove any free dyes and GO residues. After centrifugation, GO−MSNP1 was well-dispersed in H_2O at pH 6.5. The HR-TEM image of GO−MSNP1 (Figure 1c) provides clear evidence for the encapsulation of the dye and the complete wrapping of GO sheets around the MSNPs. On the basis of a comparison with the TEM image of GO−MSNP, loading of **1** in the mesopores of MSNPs apparently masks the visibility of the mesoporous structures of GO−MSNP1. SAED analysis of the GO sheets on GO−MSNP1 revealed the characteristics of the ultrathin layer of GO sheets coating the NPs (Figure 1d). This is evident from the observation that for an ultrathin layer of GO sheets, the intensity of $(0\bar{1}10)$ spots appears to be more intense than that of $(1\bar{2}10)$ spots.[1a,26]

The FE-SEM images of MSNP−NH_2 (Figure 2a) and GO−MSNP1 (Figure 2b) recorded in gentle beam mode (GB-high) reveal the morphologies of GO-sheet-coated MSNPs loaded with **1**. The surface charges of GO sheets, MSNP−NH_2, MSNP1, and GO−MSNP1 were examined using ζ potential measurements in distilled H_2O to obtain more insights on GO-sheet-covered NPs (Figure 2c). GO sheets showed a negative ζ

dx.doi.org/10.1021/ja305352d | J. Am. Chem. Soc. 2012, 134, 17346−17349

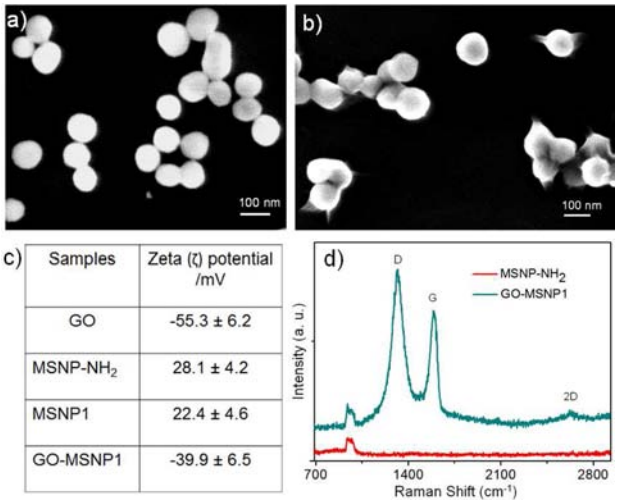

Figure 2. (a, b) Typical FE-SEM images of (a) MSNP−NH_2 and (b) GO−MSNP1. (c) Values of the ζ potential for GO sheets, MSNP−NH_2, MSNP1, and GO−MSNP1 in distilled H_2O. (d) Raman spectra of MSNP−NH_2 and GO−MSNP1.

potential of −55.3 ± 6.2 mV, indicating a negative charge over the surface of the GO sheets. MSNP−NH_2 showed a positive ζ potential of 28 ± 4.2 mV due to the amine groups on the surface. Thus, strong electrostatic interactions between the oppositely charged GO sheets and MSNP−NH_2 NPs led to the formation of GO−MSNP. **1**-loaded NPs (MSNP1) exhibited a ζ potential of 22 ± 4.6 mV, which favors GO wrapping by electrostatic interactions. GO−MSNP1 showed a negative ζ potential of −39.9 ± 6.5 mV, further confirming the surface coverage of MSNPs by negatively charged GO sheets. Figure 2d shows typical Raman spectra (λ_{ex} = 633 nm) of GO−MSNP1 and MSNP−NH_2. The Raman spectrum of MSNP−NH_2 exhibits peaks around 976 cm^{-1}, while that of GO−MSNP1 shows a combination of the characteristic peaks from GO sheets (i.e., the G band at 1593 cm^{-1} and D band at 1332 cm^{-1})[27] and MSNPs. The Raman spectra further support the wrapping of GO sheets on MSNPs.

The UV/vis spectrum (Figure 3a, red) of GO−MSNP does not show an obvious absorption at 400−700 nm in aqueous

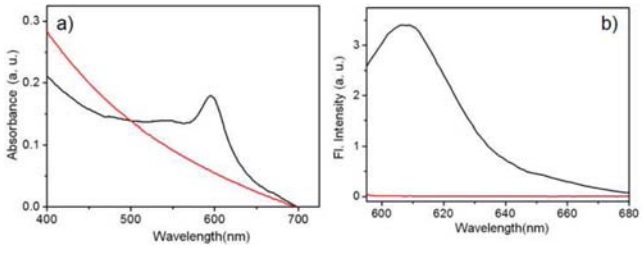

Figure 3. (a) UV/vis and (b) emission (λ_{ex} = 580 nm) spectra of GO−MSNP1 (black) and GO−MSNP (red) in aqueous solution (1 mg mL^{-1}) at pH 6.5.

solution at pH 6.5. Interestingly, under the same conditions, GO−MSNP1 (Figure 3a, black) presents a characteristic absorption maximum at 595 nm, corresponding to the absorption of **1**. Relative to the characteristic absorption maximum of free **1**, a red shift of ∼25 nm was observed for GO−MSNP1 in aqueous soluition. This observed red shift can be attributed to the encapsulation of **1** within the mesopockets of MSNPs, which is similar to the formation of a complex between the dye and serum albumin.[19]

The emission spectra of GO−MSNP1 and GO−MSNP were recorded in aqueous solution (1 mg mL^{-1}) at pH 6.5. When excited at 580 nm, GO−MSNP1 exhibits an emission with a maximum at 607 nm and a quantum yield (Φ_f) of 0.21 (Figure 3b, black), whereas GO−MSNP without the dye was found to be nonemissive (Figure 3b, red). The photophysical properties of GO−MSNP1 provide a proof of concept for the encapsulation of **1** inside the mesopores of MSNPs. The noninterfering absorption and emission bands of GO−MSNP1 under aqueous conditions make these novel NPs an excellent candidate for biological applications.

A detailed investigation of the chemical stability of GO−MSNP1 was carried out by treating the NPs with biorelevant thiol-containing molecules such as Cys and GSH. Separate sets of experiments were conducted on both free **1** (6×10^{-6} M) and freshly prepared GO−MSNP1 (1 mg mL^{-1}). The corresponding time-dependent absorption and emission changes are shown in Figure 4a,b, respectively. The reaction

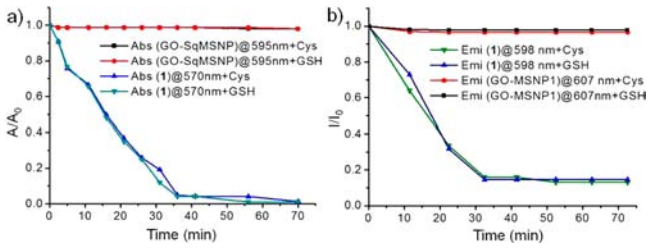

Figure 4. Changes in the (a) absorption and (b) emission of GO−MSNP1 and squaraine dye **1** upon addition of 3 mM Cys or GSH in aqueous pH 7 buffer solution at 24 °C.

of either Cys or GSH with **1** results in complete bleaching of absorption and emission at 570 and 596 nm respectively (Figure 4 and Figure S7), whereas the photophysical characteristics (absorption maximum at 595 nm and emission maximum at 607 nm) of GO−MSNP1 were found unaffected in the presence of either Cys or GSH for a substantial period of time (Figure 4). Furthermore, GO−MSNP1 is very stable, and the loaded dye does not leak out from the mesopores, since the NPs maintained all of their photophysical characteristics in aqueous solution for months. Thus, these observed results stand as a proof of concept for the protection of **1** within the mesopores in the presence of the GO sheet wrapping.

To examine the potential of GO−MSNP1 for biological applications, the inherent cytotoxicity of GO−MSNP1 was evaluated using the 3-(4,5-dimethylthiazol-2-yl)-2,5-diphenyltetrazolium bromide (MTT) viability assay with HeLa cancer cells for an incubation period of 24 h. As shown in Figure S10, GO−MSNP1 has no considerable cytotoxicity at low to moderate concentrations. We next employed GO−MSNP1 for both cell-surface and subcellular labeling to demonstrate their bioimaging ability. In vitro fluorescence imaging studies were performed with HeLa cancer cells (see the SI). Figure 5 shows the fluorescence microscopy images of HeLa cells (100× oil objective) treated with GO−MSNP1 for 24 h. The blue fluorescence from the cell nucleus stained with 4′,6-diamidino-2-phenylindole (DAPI) can be observed in Figure 5a. The red fluorescence of GO−MSNP1 is distributed inside the cytoplasm as well as on the cell surface (Figure 5b). Similarly, the overlay image (Figure 5c) indicates the accumulation of

dx.doi.org/10.1021/ja305352d | J. Am. Chem. Soc. 2012, 134, 17346−17349

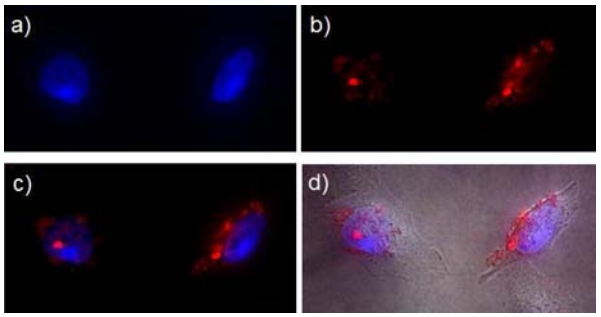

Figure 5. Epifluorescence microscopy images of HeLa cancer cells labeled with GO−MSNP1. The blue fluorescence is from the DAPI nuclear counterstain (1 μg mL^{-1}), and the red fluorescence is from GO−MSNP1. (a) Image of nuclei. (b) Fluorescence of GO−MSNP1 (dark-field). (c) Overlay of (a) and (b). (d) Overlay of (c) with the phase contrast image.

GO−MSNP1 in the cytoplasm of the cells. The overlay of Figure 5c with the phase contrast image (Figure 5d) reveals both intracellular and cell-surface labeling of GO−MSNP1. Thus, the in vitro investigations demonstrate the great potential of the novel hybrid for bioimaging applications.

In conclusion, we have developed a novel strategy for the protection of squaraine dyes by using GO-sheet-coated mesoporous silica nanoparticles, leading to a fluorescent hybrid for bioimaging applications. The ultrathin layer of GO sheets coating the dye-loaded NPs prevent both dye leakage and nucleophilic attack on the dye. The hybrid exhibits remarkable stability in aqueous solution and is biocompatible. The novel hybrid is expected to serve as a platform for a variety of biological applications, including specific in vitro and in vivo cellular imaging.

■ ASSOCIATED CONTENT

Ⓢ Supporting Information

Preparation and characterization details. This material is available free of charge via the Internet at http://pubs.acs.org.

■ AUTHOR INFORMATION

Corresponding Author

zhaoyanli@ntu.edu.sg

Author Contributions

[§]S.S. and X.M. contributed equally.

Notes

The authors declare no competing financial interest.

■ ACKNOWLEDGMENTS

We thank the Singapore National Research Foundation Fellowship (NRF2009NRF-RF001-015) and Nanyang Technological University for financial support. The assistance of Mr. P. Srikanth for SEM and Raman analysis and Ms. K. T. Nguyen for SEM analysis is gratefully acknowledged.

■ REFERENCES

(1) (a) Meyer, J. C.; Geim, A. K.; Katsnelson, M. I.; Novoselov, K. S.; Booth, T. J.; Roth, S. *Nature* **2007**, *446*, 60. (b) Neo, A. H. C.; Guinea, F.; Peres, N. M. R.; Novoselov, K. S.; Geim, A. K. *Rev. Mod. Phys.* **2009**, *81*, 109.

(2) Zhu, Y.; Murali, S.; Cai, W.; Li, X.; Suk, J. W.; Potts, J. R.; Ruoff, R. S. *Adv. Mater.* **2010**, *22*, 3906.

(3) Wang, K.; Ruan, J.; Song, H.; Zhang, J.; Wo, Y.; Guo, S.; Cui, D. *Nanoscale Res. Lett.* **2011**, *6*, 8.

(4) (a) Bi, S.; Zhao, T.; Luo, B. *Chem. Commun.* **2012**, *48*, 106. (b) Luo, M.; Chen, X.; Zhou, G.; Xiang, X.; Chen, L.; Ji, X.; He, Z. *Chem. Commun.* **2012**, *48*, 1126.

(5) Li, J.; Bao, H.; Hou, X.; Sun, L.; Wang, X.; Gu, M. *Angew. Chem., Int. Ed.* **2012**, *51*, 1830.

(6) (a) Sun, X.; Liu, Z.; Welsher, K.; Robinson, J. T.; Goodwin, A.; Zarc, S.; Dai, H. *Nano Res.* **2008**, *1*, 203. (b) Liu, Z.; Robinson, J. T.; Sun, X.; Dai, H. *J. Am. Chem. Soc.* **2008**, *130*, 10876. (c) Yang, X.; Zhang, X.; Liu, Z.; Ma, Y.; Huang, Y.; Chen, Y. *J. Phys. Chem. C* **2008**, *112*, 17554.

(7) (a) Popat, A.; Hartono, S. B.; Stahr, F.; Liu, J.; Qiao, S. Z.; Lu, G. Q. *Nanoscale* **2011**, *3*, 2801. (b) Manzano, M.; Vallet-Regí, M. *J. Mater. Chem.* **2010**, *20*, 5593.

(8) (a) Ambrogio, M. W.; Thomas, C. R.; Zhao, Y. L.; Zink, J. I.; Stoddart, J. F. *Acc. Chem. Res.* **2011**, *44*, 903. (b) Cotí, K. K.; Belowich, M. E.; Liong, M.; Ambrogio, M. W.; Lau, Y. A.; Khatib, H. A.; Zink, J. I.; Khashab, N. V.; Stoddart, J. F. *Nanoscale* **2009**, *1*, 16.

(9) (a) Lin, Y.; Tsai, C.; Huang, H.; Kuo, C.; Hung, Y.; Huang, D.; Chen, Y.; Mou, C. *Chem. Mater.* **2005**, *17*, 4570. (b) Lu, C.; Hung, Y.; Hsiao, J.; Yao, M.; Chung, T.; Lin, Y.; Wu, S.; Hsu, S.; Liu, H.; Mou, C.; Yang, C.; Huang, D.; Chen, Y. *Nano Lett.* **2007**, *7*, 149.

(10) (a) Liong, M.; Liu, J.; Kovochich, M.; Xia, T.; Ruehm, S. G.; Nel, A. E.; Tamanoi, F.; Zink, J. I. *ACS Nano* **2008**, *2*, 889. (b) He, Q.; Shi, J.; Chen, F.; Zhu, M.; Zhang, L. *Biomaterials* **2010**, *31*, 3335.

(11) (a) Ajayaghosh, A. *Chem. Soc. Rev.* **2003**, *32*, 181. (b) Ajayaghosh, A. *Acc. Chem. Res.* **2005**, *38*, 449.

(12) (a) Ajayaghosh, A.; Arunkumar, E.; Daub, J. *Angew. Chem., Int. Ed.* **2002**, *41*, 1766. (b) Arunkumar, E.; Chithra, P.; Ajayaghosh, A.; Daub, J. *J. Am. Chem. Soc.* **2004**, *126*, 6590.

(13) (a) Terpetschnig, E.; Szmacinski, H.; Ozinskas, A.; Lakowicz, J. R. *Anal. Biochem.* **1994**, *217*, 197. (b) Renard, B.; Aubert, Y.; Asseline, U. *Tetrahedron Lett.* **2009**, *50*, 1897.

(14) Beverina, L.; Crippa, M.; Landenna, M.; Ruffo, R.; Salice, P.; Silvestri, F.; Versari, S.; Villa, A.; Ciaffoni, L.; Collini, E.; Ferrante, C.; Bradamante, S.; Mari, C. M.; Bozio, R.; Pagani, G. A. *J. Am. Chem. Soc.* **2008**, *130*, 1894.

(15) Ros-Lis, J. V.; Garcýá, B.; Jiménez, D.; Martínez-Máñez, R.; Sancenón, F.; Soto, J.; Gonzalvo, F.; Valldecabres, M. C. *J. Am. Chem. Soc.* **2004**, *126*, 4064.

(16) Sreejith, S.; Divya, K. P.; Ajayaghosh, A. *Angew. Chem., Int. Ed.* **2008**, *47*, 7883.

(17) Avirah, R. R.; Jayaram, D. T.; Adarsh, N.; Ramaiah, D. *Org. Biomol. Chem.* **2012**, *10*, 911.

(18) (a) Arun, K. T.; Ramaiah, D.; Epe, B. *J. Phys. Chem. B* **2002**, *106*, 11622. (b) Arun, K. T.; Jayaram, D. T.; Avirah, R. R.; Ramaiah, D. *J. Phys. Chem. B* **2011**, *115*, 7122.

(19) Jisha, V. S.; Arun, K. T.; Hariharan, M.; Ramaiah, D. *J. Am. Chem. Soc.* **2006**, *128*, 6024.

(20) (a) Gassensmith, J. J.; Baumes, J. M.; Smith, B. D. *Chem. Commun.* **2009**, 6329. (b) Arunkumar, E.; Forbes, C. C.; Noll, B. C.; Smith, B. D. *J. Am. Chem. Soc.* **2005**, *127*, 3288.

(21) Yang, S.; Feng, X.; Ivanovici, S.; Müllen, K. *Angew. Chem., Int. Ed.* **2010**, *49*, 8408.

(22) Hummers, W. S.; Offeman, R. E. *J. Am. Chem. Soc.* **1958**, *80*, 1339.

(23) Kovtyukhova, N. I.; Ollivier, P. J.; Martin, B. R.; Mallouk, T. E.; Chizhik, S. A.; Buzaneva, E. V.; Gorchinskiy, A. D. *Chem. Mater.* **1999**, *11*, 771.

(24) Treibs, A.; Jacob, K. *Angew. Chem., Int. Ed. Engl.* **1965**, *4*, 694.

(25) Zhao, Y. L.; Li, Z.; Kabehie, S.; Botros, Y. Y.; Stoddart, J. F.; Zink, J. I. *J. Am. Chem. Soc.* **2010**, *132*, 13016.

(26) Hernandez, Y.; Nicolosi, V.; Lotya, M.; Blighe, F. M.; Sun, Z.; De, S.; McGovern, I. T.; Holland, B.; Byrne, M.; Gun'ko, Y. K.; Boland, J. J.; Niraj, P.; Duesberg, G.; Krishnamurthy, S.; Goodhue, R.; Hutchison, J.; Sacardaci, V.; Ferrari, A. C.; Coleman, J. N. *Nat. Nanotechnol.* **2008**, *3*, 563.

(27) Kudin, K. K.; Ozbas, K.; Schniepp, H. C.; Prud'homme, R. K.; Aksay, I. A.; Car, R. *Nano Lett.* **2008**, *8*, 36.